

Intelligent Wind Generator Models for Power Flow Studies in PSS®E and PSS®SINCAL

C. Opathella, *Student Member, IEEE*, B. N. Singh, D. Cheng, *Member, IEEE*, and B. Venkatesh, *Senior Member, IEEE*

Abstract—Wind generator (WG) output is a function of wind speed and three-phase terminal voltage. Distribution systems are predominantly unbalanced. A WG model that is purely a function of wind speed is simple to use with unbalanced three-phase power flow analysis but the solution is inaccurate. These errors add up and become pronounced when a single three-phase feeder connects several WGs. Complete nonlinear three-phase WG models are accurate but are slow and unsuitable for power flow applications. This paper proposes artificial neural network (ANN) models to represent type-3 doubly-fed induction generator and type-4 permanent magnet synchronous generator. The proposed approach can be readily applied to any other type of WGs. The main advantages of these ANN models are their mathematical simplicity, high accuracy with unbalanced systems and computational speed. These models were tested with the IEEE 37-bus test system. The results show that the ANN WG models are computationally ten times faster than nonlinear accurate models. In addition, simplicity of the proposed ANN WG models allow easy integration into commercial software packages such as PSS®E and PSS®SINCAL and implementations are also shown in this paper.

Index Terms—Artificial neural networks, power distribution systems, power flow, wind power generators.

NOMENCLATURE

P_m	Rotor mechanical power.
A	Area swept by the turbine.
ρ	Density of air.
U	Wind speed (m/s).
C_p	Power coefficient.
λ	Tip speed ratio.
$C_1 \dots C_6$	Constants.
B	Blade pitch angle.
ω_t	Turbine angular speed.

ω_r	Rotor angular speed.
R_t	Radius of the turbine.
K_g	Gear box coefficient.
$P_a, P_b, P_c, [P]_{abc}$	Three-phase WG real power output.
$Q_a, Q_b, Q_c, [Q]_{abc}$	Three-phase WG reactive power output.
$V_a, V_b, V_c, [V]_{abc}$	Magnitudes of three-phase voltage at PCC.
$\delta_a, \delta_b, \delta_c, [\delta]_{abc}$	Angles of three-phase voltage at PCC.
$[V \angle \delta]_{abc}$	Three-phase voltage at PCC.
$[P]_{sabc}, [Q]_{sabc}$	Real and reactive power supply from stator to PCC.
P_{s0}, P_{s1}, P_{s2}	Stator power at different symmetrical component networks.
$\bar{I}_{s0}, \bar{I}_{s1}, \bar{I}_{s2}$	Stator winding current phasors at different symmetrical component networks.
Z_{s0}, Z_{s1}, Z_{s2}	Symmetrical component stator winding impedances.
$\bar{V}_{s0}, \bar{V}_{s1}, \bar{V}_{s2}$	Stator voltage phasors at different symmetrical component networks.
P_{r0}, P_{r1}, P_{r2}	Rotor power at different symmetrical component networks.
$\bar{I}_{r0}, \bar{I}_{r1}, \bar{I}_{r2}$	Rotor winding current phasors at different symmetrical component networks.
Z_{r0}, Z_{r1}, Z_{r2}	Symmetrical component rotor winding impedances.
$\bar{V}_{r0}, \bar{V}_{r1}, \bar{V}_{r2}$	Rotor voltage phasors at different symmetrical component networks.
$[P]_{gabc}, [Q]_{gabc}$	Real and reactive power supply from grid side converter to PCC.
$\bar{E}_0, \bar{E}_1, \bar{E}_2$	Induced emf phasors at different symmetrical component networks.
$s_0, s_1, s_2, [s]_{012}$	Converted symmetrical component slip.
s	Machine slip.

Manuscript received January 26, 2012; revised May 14, 2012 and June 27, 2012; accepted July 26, 2012. Date of publication September 13, 2012; date of current version April 18, 2013. This work was supported in part by the Hydro One grant and NSERC grants awarded to B. Venkatesh. Paper no. TPWRS-00026-2012.

C. Opathella, D. Cheng, and B. Venkatesh are with the Centre for Urban Energy, Ryerson University, Toronto, ON M5B 2K3, Canada (e-mail: bala@ryerson.ca).

B. N. Singh is with Hydro One Networks Inc., Toronto, ON M5G 2P5, Canada (e-mail: bob.singh@hydroone.com).

Color versions of one or more of the figures in this paper are available online at <http://ieeexplore.ieee.org>.

Digital Object Identifier 10.1109/TPWRS.2012.2211043

$Z_{m0}, Z_{m1}, Z_{m2}, [Z]_{m012}$	Symmetrical component magnetizing reactance with respect to stator of the machine.
Z_m	Magnetizing reactance with respect to stator of the machine.
ε	Index to denote the symmetrical component network.
PL_0, PL_1, PL_2	Stator and rotor copper losses in sequence networks.
Er	Derivative of the error power.
$f(\cdot)$	Sigmoid activation function.
ns	Net-stimulus.
T	Output layer of the neural network.
i, j	Index to specify the neurons.
k	Index to specify the layer.
x	Normalized output of a neuron.
y	Normalized target output of a neuron.
X	Non-normalized output of a neuron.
Y	Non-normalized target output of a neuron.
w	Weights of links.
η	Leaning rate.
MAE	Maximum absolute error.
AAE	Average absolute error.
Ne	Number of epochs.
N_{out}	Number of output neurons in the output layer.
$ARMSE$	Average root mean square error.
e	Index to specify epochs.

I. INTRODUCTION

ENVIRONMENTAL awareness has triggered a number of government programs to harness green energy. Different forms of the feed-in-tariff (FIT) programs exist in many countries to provide financial incentives for stimulating widespread installation of renewable generators. As a result, a large number of wind generators (WGs) are being connected to distribution systems (DSs). Unique characteristics of DSs (as opposed to transmission systems) are 1) their radial or weakly meshed configuration, 2) unbalanced lines and loads, and 3) their high R/X ratio [1], [2], [4], [5]. Therefore DS power flow studies are carried out considering the three-phase system. All network components have to be modeled accurately considering unbalanced three-phase system.

A. Power Flow Analysis With Wind Generators

The simplistic PQ modeling approach was shown to be satisfactory in representing WGs when a very few of them of small sizes were connected to a DS and the DS is balanced three-phase system. Hence simple (inaccurate) representation of WGs using PQ values, as a function of wind speed without accounting voltage unbalances at the point of connection with DS, did not significantly influence power flow analysis results of DSs. Therefore, it was common that the outputs of WGs were assumed constant for a given wind speed. Even though the output power of WG depends on the voltage at point of common coupling (PCC), in most power flow studies, WGs were modeled as simple fixed power injections (independent from the terminal voltage) and purely a function of wind speed [2], [3].

With increased proliferation of several large sized WGs in DSs with many on the same feeder, numerous instances are found where WGs comprise the major portion of power flow in the DS and at times causing reverse power flow from DS into the transmission system (TS). This simple (inaccurate) representation of WGs using PQ values, as a function of wind speed, is inadequate to provide accurate results for distribution system analysis when several and larger machines are connected and the DS is considerably unbalanced. In such cases, accurate modeling of WGs becomes a must for accurate power flow analysis of DSs. Therefore, it is important to model unbalanced three-phase DS voltage at PCC and ensure that the WG model properly accounts for the unbalanced supply. In [4]–[17] different accurate WG models discuss the steady state behavior of WGs.

Hence, it is imperative that WGs be accurately modeled considering both wind speed and three-phase supply voltage phasors for accurate three-phase power flow analysis of DSs. A flow chart for the modified ladder iterative power flow algorithm with an accurate WG model is shown in Fig. 1.

B. Effect of Voltage Deviation

Further, it may be noted that converters of wind generators try to operate the machines such that they extract maximum power from the wind. Barring some losses, this power shall appear at the PCC as the sum of powers flowing from three phases. When the three-phase voltage at PCC is balanced and at rated value, the per phase power outputs are equal and equal to the rated power value. However, when the voltage magnitude drops, the phase currents increase and thus the total power loss in the WG also increases. Due to this effect, drop in the PCC voltage magnitude reduces the total power supply to the PCC.

Further, unbalanced PCC voltage (voltage angle deviations) causes, per phase power output to be unequal, while, the sum of per phase power to be equal to the mechanical power input from the wind turbine. These unequal power flows from the WG causes voltage regulation issues on the DS lines. An example of the extent of imbalance in phase power with angle imbalance is shown in Table I considering WG [16].

Reviewing the unbalanced case in Table I, it is obvious that representing WGs using balanced PQ values as a function of wind speed without accounting voltage unbalances at the point of connection with DS is highly inaccurate.

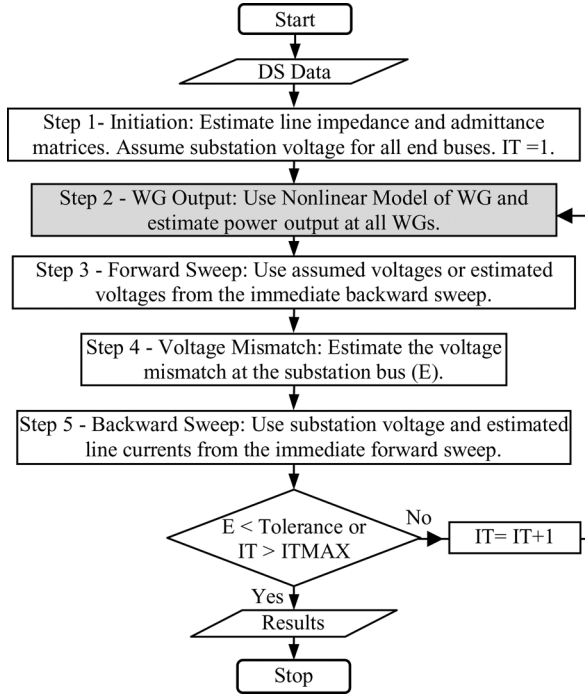


Fig. 1. Block diagram showing the Ladder Iterative Technique power flow algorithm with WG [21].

TABLE I
POWER OUTPUT VARIATIONS FOR DIFFERENT PCC VOLTAGES

Case: Balanced PCC Voltage			
	Phase a	Phase b	Phase c
Phase voltage at PCC	$0.94\angle 0^\circ$ pu	$0.94\angle -120^\circ$ pu	$0.94\angle -240^\circ$ pu
Phase Real Powers	0.8903 pu	0.8908 pu	0.8907 pu
Case: Unbalanced PCC Voltage			
Phase voltage at PCC	$0.99\angle 3^\circ$ pu	$1.06\angle -122^\circ$ pu	$0.94\angle -245^\circ$ pu
Phase Real Powers	0.2591 pu	1.0784 pu	1.3159 pu

Further, these deviations (between rated and actual) are compounded in long feeders with several WGs. This is the typical case in Northern Ontario, Canada. Therefore it is important to accurately model WGs considering the three phases accounting for their power output relationship to three-phase system voltage at PCC and wind speed.

C. Wind Generator Modeling

In [4]–[7], buses with WGs were modeled as constant power, constant power factor, or constant voltage nodes with required modifications to capture the characteristics of the WGs. The authors of [8]–[17] model the WG by cascading the turbine, the induction/synchronous generator and the power converter models. The nonlinear relationship between wind velocity and power output of turbines was used in these WG models. In [16] and [17], the authors developed nonlinear models for the DFIG and the PMSG WGs respectively by modeling each WG component. These two models have a three-phase representation of WG that consider unbalanced DS voltage at PCC and mutual admittances.

There are four main types of WGs. Two of them, namely the Type-3 doubly-fed induction generator (referred to as the DFIG) and the Type-4 full capacity converter connected permanent

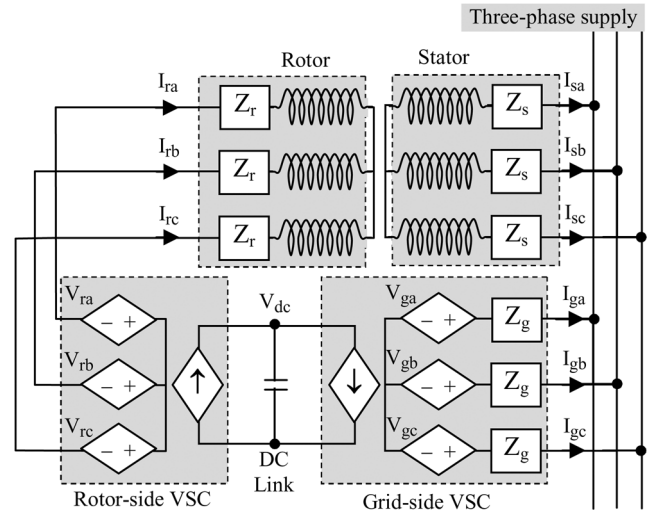


Fig. 2. Equivalent circuit diagram of doubly-fed induction generator—complete model.

magnet synchronous generator (PMSG) have become popular due to their characteristics. In industry, both synchronous machines and induction machines are used for Type-4 WGs. Power output of these WGs is a function of wind speed and voltage at PCC. Research on this subject reveals that estimating the power output of a WG requires knowledge of seven parameters: the wind velocity, and the three WG terminal voltage magnitudes and respective phase angles. The relationship between these parameters and the WG output power are highly nonlinear, as explained in [8]–[17].

The block diagram of the type-3 DFIG WG's nonlinear model [16] is shown in Fig. 2. The mathematical model for type-3 DFIG WG is given in Appendix A. A complete model for type-4 PMSG is given in [17]. The complete nonlinear mathematical model of any type of WG can be represented as below using matrix equations where three-phase PCC voltage and wind speed are related to net real and reactive power injections from the WG into the connected bus (A23):

$$0 = F[U, [V]_{abc}, [\delta]_{abc}, [P]_{abc}, [Q]_{abc}]. \quad (1)$$

Here F is a multidimensional matrix equation comprising a set of nonlinear equations.

Generally these models (1) are nonlinear due to the nature of the machine. Therefore, Newton-Raphson technique is popularly used to solve these models. It is an iterative technique and needs to be solved for each connected WG in DS in every power flow iteration (Fig. 1). Therefore, these nonlinear WG models, when integrated in power flow algorithms, result in slow convergence, considerably slowing down the power flow solution [12]. Furthermore, industries and utilities use commercial software such as PSS@E and/or PSS@SINCAL where integration of such iterative solution of nonlinear models is not possible.

D. Proposed Work

To overcome the challenge of higher computational effort, solution time and difficulty to incorporate them readily to commercial software, the use of artificial neural network (ANN) to model WG is proposed in this paper. The use of ANN in

wind power is not new but in most cases ANN is deployed for forecasting wind power [18]. In such studies econometric models are replaced by ANNs. However, this paper proposes three-phase WG models using ANN to replace the existing nonlinear WG models. The proposed ANN models for WGs emulate (1), the nonlinear three-phase WG models that are functions of wind speed and three-phase PCC voltage (1).

In contrast to the nonlinear models, ANN models develop an empirical mapping of the input-output relationship using a given input-output data (Epochs) set. If the accurate nonlinear model for a WG is available, it can be used for generating epochs or otherwise metered data of a WG can be used as epochs. This aspect of using metered data for modeling a WG is a huge benefit of the proposed method. The process of generating epochs and building ANN WG models are explained in detail in the following sections of this paper. The proposed ANN models are computationally much faster than the corresponding nonlinear WG models, and can be easily extended for modeling wind farms by accounting several wind speeds. This means ANN approach provides a universal WG modeling technique which can be used to model any type or size of WG or wind farms. In addition the proposed ANN WG model reduces the convergence time of DS power flow studies while maintaining accuracy. Further, if there are several wind generators or farms in the system, as the case might be in a transmission system, the computational benefits are significant. The other advantage of the proposed ANN WG model is that it can be easily implemented in commercial software packages such as PSS®E and PSS®SINCAL irrespective of size/type of the WG because they use linear matrix relationships.

Through the ANN model developed in this paper maps nonlinear WG models of type-3 DFIG and type-4 PMSG developed in [16] and [17], respectively, the proposed ANN WG model is equally suitable to replace any other nonlinear wind generator model.

The paper is organized as follows. Section II provides a brief introduction to ANNs. In Section III, ANN WG models for type-3 DFIG and type-4 PMSG are developed and in Section IV they are tested on a three-phase DS power flow program. Section V provides a case study where ANN WG models were implemented in PSS®E and PSS®SINCAL. Section VI concludes the paper.

II. ARTIFICIAL NEURAL NETWORK APPROACH

A typical feed-forward neural network model (back propagation network—BPN) is used to model WGs in this paper. Sample architecture is shown in Fig. 3.

In this work, k is used as a notation for the k th layer of an ANN. There can be N_k neurons in any hidden layer. The number of neurons in the input and output layers are determined by the number of input and output variables of the WG's nonlinear model (1). The number of hidden layers and the number of neurons in each hidden layer are determined by experimenting with available data set. This experimentation process and the selection criterion are explained at the end of this section. A neuron is formed by one or more inputs, a functional element and an output. Fig. 4 shows a neuron and its notation as employed in this paper.

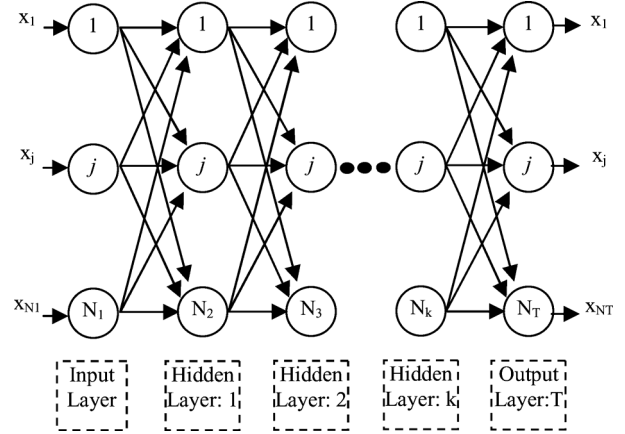


Fig. 3. Generic ANN architecture.

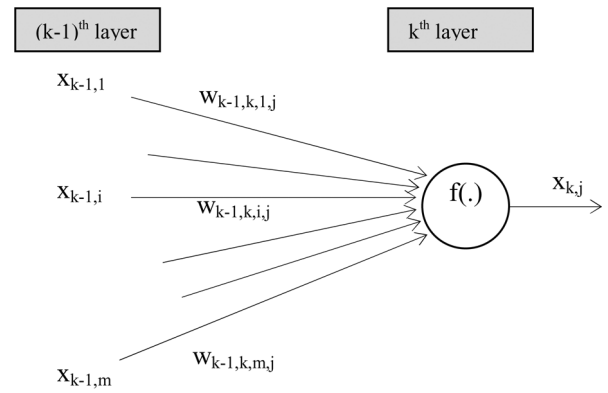


Fig. 4. Neuron and its notation in an ANN model.

The back propagation network (BPN) algorithm is explained in Appendix B [19] and it was used for the ANN WG models developed in this paper. In this notation, $w_{k-1,k,i,j}$ represents the weight of the link between the i th neuron in $(k-1)$ th layer and the j th neuron in k th layer. The variable $w_{k-1,k,0,0}$ represents the bias value of layer k . The output of the neuron i in layer $(k-1)$ is denoted by $x_{k-1,i}$. The total input signal into the j th neuron of layer k is the net-stimulus ($ns_{k,j}$) and it is the weighted summation of outputs of m neurons in the layer $(k-1)$:

$$ns_{k,j} = w_{k-1,k,0,0} + \sum_{i=1}^m w_{k-1,k,i,j} \cdot x_{k-1,i}. \quad (2)$$

The output of the neuron j in layer k is written as

$$x_{k,j} = f_{k,j}(ns_{k,j}). \quad (3)$$

The sigmoid activation function of the neuron j in layer k is denoted by $f_{k,j}(\cdot)$. The feed-forward neural network (Fig. 3) is completely trained to estimate all the weights using BPN algorithm given in Appendix B.

III. ARTIFICIAL NEURAL NETWORK MODELS OF WGS

In order to build an ANN, it is necessary to identify the input and output variables. Seven parameters are available to estimate the power output of a WG. These are wind speed and PCC voltage: U , V_a , V_b , V_c , δ_a , δ_b , and δ_c . In the ANN framework, these are called input variables. These inputs are fed to the input

layer of the neural network. The outputs of the neural network are the three phase powers (real and reactive) being delivered by the WG at the PCC to the distribution system. The output, therefore, consists of six variables representing the real and reactive powers from each of the three phases (P_a , P_b , P_c , Q_a , Q_b , and Q_c). These output variables represent the output layer of the neural network. In sections below, the process of building and testing, ANN Models of DFIG Type-3 WG and PMSG Type-4 WG are described.

A. ANN Model for Type-3 DFIG WG

To create an ANN model, it is required to train a neural network using a sample input-output data set (epochs) until it gives the accurate answer. In this study, sample input/output epochs were created using nonlinear model (A23).

The input data for the ANN model of the type-3 DFIG WG comprises: U , V_a , V_b , V_c , δ_a , δ_b , and δ_c . The three series were created by taking 10 000 random numbers between 0.94 pu and 1.06 pu, one for each voltage magnitude for phases a, b, and c. Three more series of 10 000 random data points were chosen in the range of -5° to 5° , one series each for voltage phase angles for phases a, b, and c. In addition to that, a series of 10 000 random numbers between 4 m/s and 20 m/s was chosen as wind speed data. Using the above mentioned input data series, output data series is computed. Computing the output data series depends on the type of WG model that is being modeled. This work considers the Type-3 DFIG WG shown in Fig. 2 and modeled using (A23) of Appendix A. Solving this model once for every data set using Newton-Raphson technique yielded corresponding output data: P_a , P_b , and P_c . Min-Max data normalization technique was used to normalize inputs and outputs for training ANNs.

The ANN model training algorithm explained in Appendix B was programmed in Matlab environment. This program was used for training the ANN model of type-3 DFIG WGs. The convergence of weights was investigated by the evaluating maximum absolute error (MAE) (B4) and average absolute error (AAE) (B5) using normalized outputs. After training numerous neural networks of different configurations (hidden layers and neurons in each layer) using the program, the configuration having the smallest average root mean square error (ARMSE) (B6) was selected.

The smallest ARMSE was found to be 0.0138 for an ANN consisting of four-layers. The configuration consists of seven neurons in the input layer (three-phase voltages phasors and the wind speed), ten neurons in the first hidden layer, ten neurons in the second hidden layer and three neurons in the output layer representing the three-phase real power output of the WG. The bias values at each layer are 0.0, -0.5 , -1.0 , and -1.8 , respectively. The variation of AAE (B5) for this ANN is shown in Fig. 5.

The graph in Fig. 5 is for the chosen configuration of ANN model of type-3 DFIG WG. It shows reduction in the AAE with training. It also shows that it is fully trained for 1000 epochs within 1000 iterations and the deviation from the nonlinear model (A23) is minimal. This ANN model, being a feed forward network, hold a set of matrices and it easily

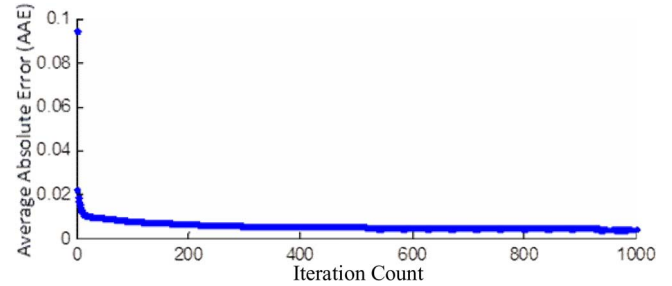


Fig. 5. Reduction of absolute error over the number of iterations.

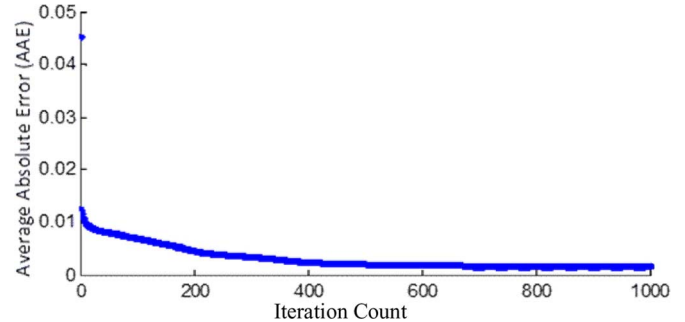


Fig. 6. Reduction of absolute error over the number of iterations.

implementable in PSS@E or PSS@SINCAL type commercial programs for power flow analysis.

B. ANN Model for Type-4 PMSG WG

As explained in the preceding section, the same set of random input variable series (U , V_a , V_b , V_c , δ_a , δ_b , and δ_c) was considered for building ANN model of type-4 PMSG WG. Using the Type-4 PMSG WG model in [17], real power output series (P_a , P_b , and P_c) was computed. It helped to create a set of 10 000 epochs. After training several ANN configurations, the configuration with the lowest ARMSE (B6) with a value of 0.0014 was selected. The selected configuration of ANN model for Type-4 PMSG WG has four layers. The input layer and the output layer have seven and three neurons respectively. Both hidden layers have ten neurons each. The variation of AAE (B5) of the selected ANN configuration during the training process is shown in Fig. 6.

The graph shows that the ANN model of PMSG WG is fully trained for the 1000 epochs within 1000 iterations and the deviation from the nonlinear model (A23) is minimal. This ANN model is readily implementable in commercial programs such as PSS@E or PSS@SINCAL for power flow analysis.

C. ANN Configurations and Effect of Learning Rate

The smallest ARMSE was the criterion for selecting the best ANN configuration. Coincidentally, ARMSE, AAE and MAE shows very similar pattern of variation. Both in ARMSE and AAE, the output error is averaged over the number of output neurons and number of epochs as given in (B5) and (B6). But MAE (B4) gives the maximum absolute error at any output at any epoch without any averaging effect. Therefore MAE gives

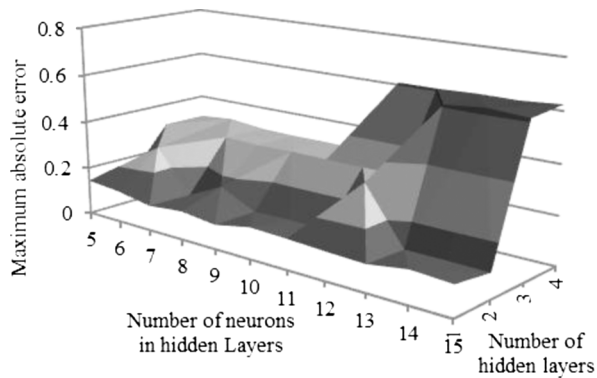


Fig. 7. MAE of different ANN configurations—type-3 DFIG WG model.

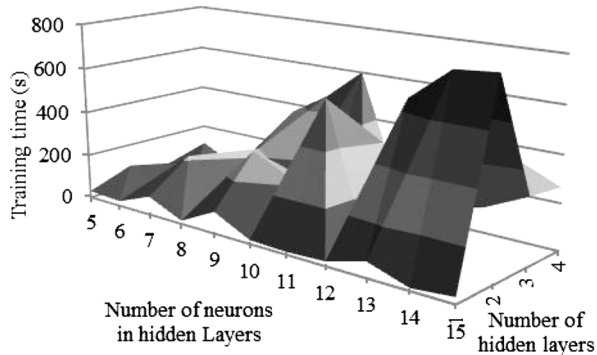


Fig. 8. Convergence time of different ANN configurations of type-3 DFIG WG.

closest picture of the trained ANN's accuracy. Accordingly, effect of network configurations and learning rate on MAE and training time was analyzed for the ANN model of type-3 DFIG WG and is reported below. A similar analysis on the ANN model of type-4 PMSG WG was completed and results were found to be similar.

1) *Effect of ANN Configuration on Accuracy:* In this study, MAE was plotted to select the best ANN configuration. Fig. 7 shows the MAE of different ANN configurations. On reviewing Fig. 7, the ANN configuration with two hidden layer and 10 neurons each has the lowest MAE and is selected for the proposed type-3 DFIG WG model.

2) *Effect of ANN Configuration on Training Time:* Apart from the accuracy of ANN, time taken for the convergence was also studied. Fig. 8 shows convergence time required with different ANN configurations. Training convergence was decided with MAE tolerance of 0.0001 and learning rate 0.7. Generally, when the ANN configuration is complex (many hidden layers and neurons) the convergence time is higher. However, there are exceptional larger configurations that train faster than smaller sized configurations.

3) *Effect of Learning Rate on Training Time:* The learning rate (η) and the MAE tolerance have a direct relationship to the training time of ANN. In order to investigate this relationship, the selected ANN configuration (2 hidden layers with 10 neurons each) was trained with different learning rates and tolerance criteria. The results of this study are given in the Fig. 9. According to the analysis, it is clear that when the optimum

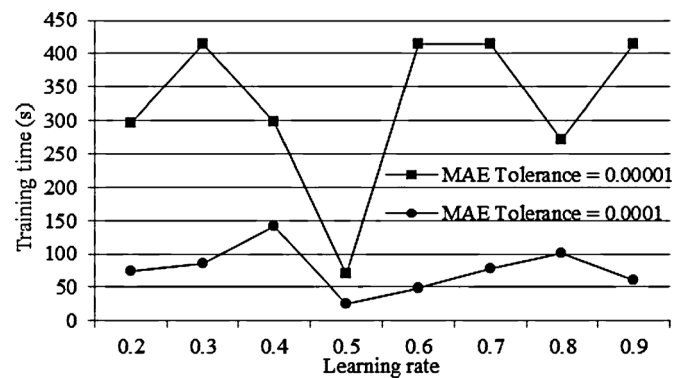


Fig. 9. Convergence time of the selected ANN configuration of type-3 DFIG WG for different learning rates and convergence criteria.

learning rate (0.5) is selected, this ANN can be trained considerably faster even for a tighter convergence criterion.

From ANN modeling study, it was noticed that, as the number of epochs is increased for detailed modeling of WG, the ANN WG model remains model size invariant. Further, the ANN WG model provides continuous mapping as it interpolates its training epoch set.

IV. DISTRIBUTION SYSTEM POWER FLOW STUDY WITH TYPE-3 AND TYPE-4 ANN WG MODELS

Successful training in Sections IV.A and IV.B show that the proposed ANN models accurately map the nonlinear models of WG, (A23) and [17] for type-3 DFIG and type-4 PMSG. In this section, we test the performance of the proposed ANN WG models in power flow analysis. Even though we implement these proposed ANN models in the modified ladder iterative technique, they equally suitable to use with other methods of power flow analysis.

The IEEE 37-bus test distribution system [20], shown in Fig. 10, was used to assess the performance of the proposed ANN models of type-3 DFIG and type-4 PMSG WGs. This test system is an unbalanced three-phase distribution system with unbalanced loads and underground cables. The power balance equations were solved using the ladder iterative technique [21] (Fig. 1). All the unbalanced network components were modeled accurately considering their mutual couplings and capacitance elements. In accurate three-phase power flow studies, WGs have to be modeled accurately considering all the three phases. In order to check performance of different WG models, two separate distribution system power flow studies (Study 1 and Study 2) were completed in Matlab considering type-3 DFIG WG and type-4 PMSG WG models, respectively. In each power flow study, the proposed ANN WG models were compared with corresponding traditional fixed PQ WG model and with corresponding nonlinear model to assess the accuracy of the proposed model and solution. In both studies it is assumed that a WG is connected to bus 775 and that the rating of the transformer XFM-1 connected between bus 775 and 709 was modified to match the power generation from the WG. In order to magnify the effects of the wind generator, a 1.0-MW per-phase pure active power load was added at buses 730 and 731. These assumptions are similar to those of [16] and

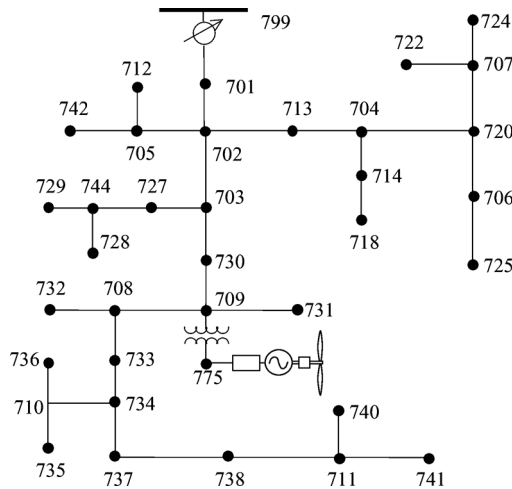


Fig. 10. Wind generator connection to the IEEE 37 three-phase distribution system.

[17]. Both the ANN and the nonlinear WG models that estimate power output are functions of wind speed and three-phase PCC voltage phasors. For fixed PQ models, the power output is estimated externally using the power output curves supplied by the WG manufacturer for the operating wind speed and is not a function of PCC voltage. For these power flow studies, the wind speed was assumed equal to 14 m/s for all models.

A. Study 1: IEEE 37-Bus System With Type-3 DFIG WG

The details for this power flow study include: 1) the capacity of the transformer XFM-1 was taken as 1.5 MVA (0.5 MVA in original IEEE 37-bus test system) and the same was considered as the system MVA base, 2) the transformer low voltage side is taken to be 2.4 kV (0.48 kV in original IEEE 37-bus test system). This data is same as that used in [16]. Three cases with different type-3 DFIG WG models were considered:

Case 1 is a power flow study using the nonlinear DFIG WG model described in (A23) and [16]. The WG is assumed to operate at unity power factor.

Case 2 is a power study using, a fixed PQ model having negative real power load of 0.8916 pu for all three-phases. Reactive power injection was assumed zero for all three phases.

Case 3 is a power flow study using the proposed ANN type-3 DFIG WG model explained Section III. This ANN model mimics unity power factor operation of the nonlinear model [16].

Except for the WG models, all other values were the same in all three cases. Wind speed is 14 m/s for all three cases. The nonlinear WG model (i.e., model used in Case 1) is considered as the most accurate because it has no approximations [16]. Therefore, Case 1 was used as the basis for the comparison with the other two cases. The accuracy of the power flow solution using the proposed ANN model was compared with Case 1, revealing a close match of results. Fig. 11 shows the deviations of voltage solutions of Cases 2 and 3 of power flow study 1 compared to the voltage solution of Case 1. From the graph (Fig. 11), it can

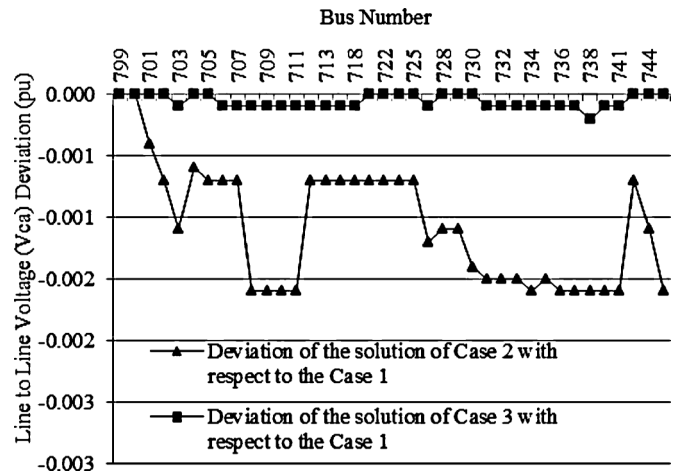


Fig. 11. Study 1: case 2 (PQ model) and case 3 (ANN model) bus voltage deviations from the voltage solution of case 1 (accurate nonlinear model).

TABLE II
EXECUTION TIMES WITH TYPE-3 DFIG WG MODELS

	Fixed PQ	Nonlinear	ANN
Time taken for executing the model once (ms)	0.0020	59.9713	4.9915
Number PF iterations	10	11	10
Average execution time taken for the PF study (s)	0.9831	1.8789	1.1302

be clearly noted that power flow results of Case 3 with ANN model of DFIG WG, are in very good agreement with those of Case 1 with the nonlinear WG model. In contrast, Case 2 with the fixed PQ model gives the larger error as compared to Case 1. These power flow solution errors are the result of inaccurate estimates of WG model's real power output. Fixed PQ model has the highest real power output errors compared with real power output of nonlinear model. They are 10%, 2%, and 6% in P_a , P_b , and P_c respectively. Observed real power output estimation errors in ANN WG model are 0%, 2%, and 0% in P_a , P_b , and P_c , respectively. This clearly shows that even though the errors in the voltage solution are small, the corresponding real power solution is significantly inaccurate.

The main advantage of the ANN-based approach is its high accuracy which is comparable to that of the nonlinear models while it greatly surpasses the nonlinear models in computational speed. Table II shows that the fixed PQ models have the fastest execution times because the PF reads those models by loading a simple data file with no further computation. While the ANN model of type-3 DFIG WG has the second best execution time, the nonlinear models have the slowest execution time. Comparing the execution times, it is noted that the ANN model of type-3 DFIG WG is twelve times faster than the nonlinear model. This leads to a much faster solution of the power flow study. In the study 1, the total execution time was improved by about 40% when the ANN model is used instead of nonlinear model. Even though the improvement may seem to be moderate in absolute terms for this simple system with one WG, the improvement will be significant when solving power flow problems of large systems with several WGs.

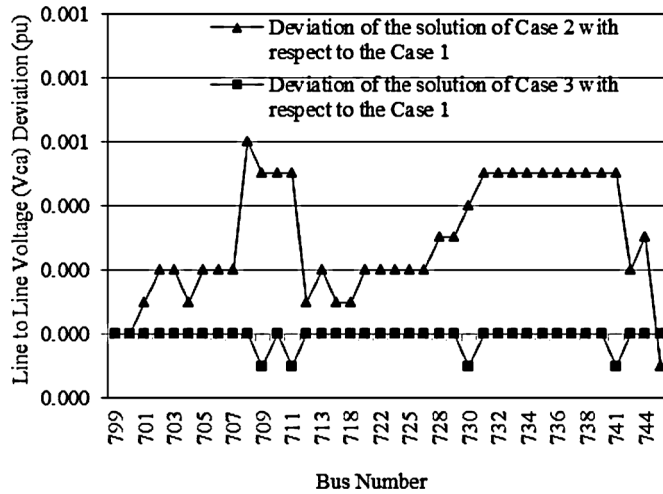


Fig. 12. Study 2: case 2 (PQ model) and case 3 (ANN model) bus voltage deviations from the voltage solution of case 1 (accurate nonlinear model).

B. Study 2: IEEE 37-Bus System With Type-4 PMSG WG

The details of this power flow study are as follows [17]: 1) the capacity of the type-4 PMSG WG, system power base and the rating of XFM-1 are 2 MVA, 2) the generation voltage is 575 V (the low side voltage rating of XFM-1).

Similar to the previous comparison, three cases were considered with different type-4 PMSG WG models and the results are compared. Wind speed is 14 m/s for all three cases below.

Case 1 is a power flow study using the accurate nonlinear WG model described in [17]. Reactive power supply is assumed zero for all three phases.

Case 2 is a power flow study using, a fixed PQ model having negative real power load of 1.0 pu for all three phases. Reactive power injection was assumed zero for all three phases.

Case 3 is a power flow study with the proposed ANN type-4 PMSG WG model explained Section III. This ANN model mimics the unity power factor operation of nonlinear model of [17].

Fig. 12 shows the deviations of voltage solutions of Cases 2 and 3 of power flow study 2 compared to the voltage solution of Case 1, which is the most accurate solution. It can be clearly seen that power flow results of Case 3 using ANN model of type-4 PMSG WGs is in very good agreement with accurate results of Case 1 using the nonlinear WG models (Fig. 12). In contrast, Case 2 with the fixed PQ models give the larger error as compared to Case 1.

Per phase real power output estimation errors in P_a , P_b , and P_c (compared with nonlinear model) are: 6%, 4%, and 2%, respectively, for the fixed PQ model, and 2%, 1%, and 1% for the ANN WG model. On making time based performance comparison, the proposed ANN model for type-4 PMSG WG is much faster than the corresponding nonlinear model, Table III.

V. IMPLEMENTATION IN COMMERCIAL SOFTWARE PACKAGES

From Figs. 11 and 12 and Tables II and III, it can be seen the ANN models of type-3 DFIG and type-4 PMSG WGs are

TABLE III
EXECUTION TIMES WITH PMSG TYPE-4 WG MODELS

	Fixed PQ	Nonlinear	ANN
Time taken for executing the model once (ms)	0.0020	66.5356	3.4714
Number of PF iterations	10	10	10
Average execution time taken for the PF study (s)	1.002325	1.844308	1.028588

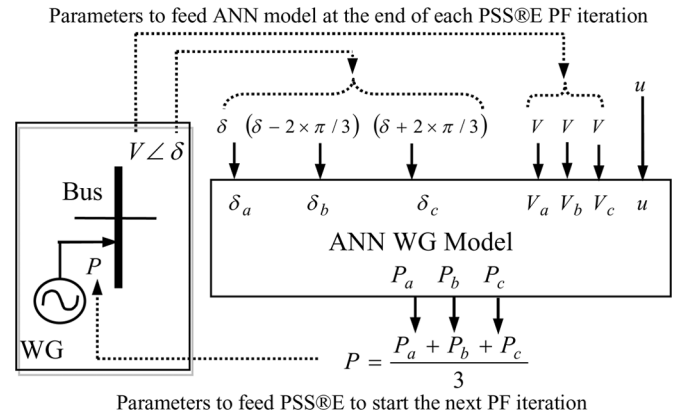


Fig. 13. Snapshot of each PSS@E PF iteration.

as accurate as nonlinear models and much faster than the nonlinear models. Further, as shown above, the ANN model can be built for any type/size of wind turbine/farm without extra effort. The only requirement is the complete data set explained in Section IV.

An important benefit of the proposed ANN models of WGs is that their ready integration into popular commercial power system analysis software. To investigate the flexibility of implementation in commercial power flow software, the ANN model of type-3 DFIG WG explained in Section IV was coded using python script language in Power System Simulator for Engineers (PSS@E) software. The PSS@E is a transmission system planning tool which calculates network states assuming the single line equivalent network. But the ANN type-3 DFIG WG model described in Section IV was built considering a three-phase system. To overcome this incompatibility a positive sequence phasor system was generated using the voltage solution of PSS@E power flow iteration. Then the generated positive sequence voltage phasor system was fed to the ANN model of type-3 DFIG WG. At end of each power flow iteration, bus voltages are updated and hence the power output from the wind turbine is updated (Fig. 13). The ANN model of type-3 DFIG WG described in Section VI was implemented in a hypothetical test system which signifies the effect of WG. This implementation was verified by establishing identical results in Matlab environment using ANN model of type-3 DFIG WG. The Fig. 14 shows variation in the output of the ANN model of type-3 DFIG WG with PSS@E voltage solution. The power flow solution process converged and the ANN model of type-3 DFIG WG stabilized at 0.8908 pu as its active power output.

The same ANN model of type-3 DFIG WG was implemented in PSS@SINCAL, which can solve three-phase unbalanced distribution system power balance equations. The ANN model of type-3 DFIG WG was coded as a Windows Script macro

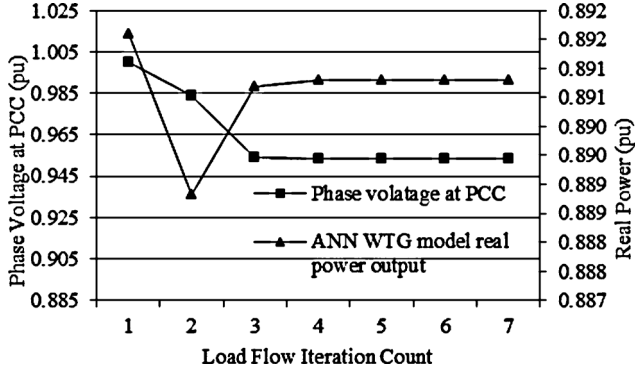


Fig. 14. Variation of real power output of ANN WG model in PSS@E.

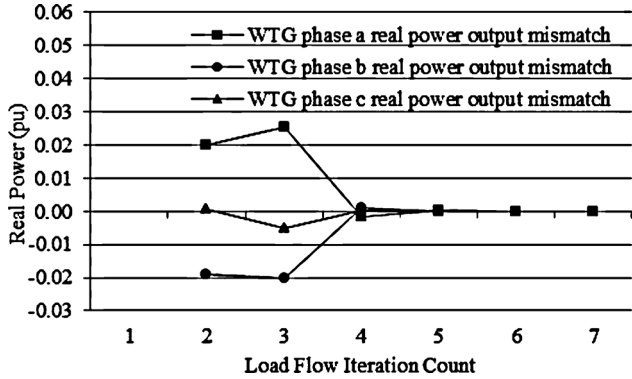


Fig. 15. Variation of three-phase real power output mismatch of ANN WG model in PSS@SINCAL.

in PSS@SINCAL. The real power output mismatch of ANN model of type-3 DFIG WG at the end of each power flow iteration is shown in Fig. 15. When the voltage solution converges, the output of the ANN model also stabilizes and mismatch approaches zero. These implementations are possible because the ANN model does not require any complex solvers or optimization techniques to estimate the power outputs.

These implementations proved the simplicity of adopting the ANN models of WGs for any practical power flow study. It further reveals that the ANN model of type-3 DFIG WG can be adapted to any system, even for those where actual manufacturer data is not available. In that case the ANN model of type-3 DFIG WG is built using the measured inputs-outputs of the wind generator and integrated into the power flow analysis software using simple programming code.

Further, it is important to point out that, on testing the proposed ANN WG model, it has not caused any algorithmic stability issues with the Ladder Iterative Technique or other power flow solution techniques used in PSS@E and PSS@SINCAL.

VI. CONCLUSION

This paper reports the development of ANN-based models of type-3 DFIG and type-4 PMSG WGs, test their performance and demonstrates their ready integration into popular commercial power system analysis software. These ANN models are: 1) accurate three-phase models as the true nonlinear models that are functions of wind speed and terminal voltage phasors, 2) suitable for unbalanced three-phase systems, 3) much faster than

conventional nonlinear models, 4) universal hence they can be trained to model any type/size of WGs, 5) readily extendable to model WGs without nonlinear models using measured data, and 6) easily extendable for modeling wind farms.

The proposed ANN models are trained using accurate models of WGs and implemented in power flow algorithms in Matlab, PSS@E and PSS@SINCAL.

Comparing accuracy of results of the power flow studies with fixed PQ models that are a function of wind speed, nonlinear accurate models and ANN models, it can be seen that ANN models give very accurate solutions that are very close to those of the nonlinear models. Furthermore, ANN WG models are computationally ten times faster than nonlinear WG models. The fast execution of ANN WG models improve the overall execution time of power flow algorithm by at least 40%, as demonstrated when testing with a small distribution system with one WG. This improvement will be very significant for larger systems with several WGs.

As a further contribution of this paper, these ANN WG models have been demonstrated to be easily implemented in commercial software packages such as the PSS@E and PSS@SINCAL which only require minimal integration effort entailing only a few lines of coding. The results from these commercial software packages thus evidently prove the feasibility of applying the proposed ANN models to practical engineering power flow studies.

APPENDIX

A. Nonlinear Mathematical Model of Type-3 DFIG WG [16]

Mechanical power of the turbine is given as

$$P_m = \frac{1}{2} \cdot A \cdot \rho \cdot U^3 \cdot C_p \quad (A1)$$

where

$$C_p(\lambda, \beta) = C_1 \left(\frac{C_2}{\lambda} - C_3 \cdot \beta - C_4 \right) \times \exp\left(\frac{-C_5}{\lambda}\right) + C_6 \cdot \lambda. \quad (A2)$$

The turbine and the rotor angular speeds are given as

$$\omega_t = \frac{\lambda \cdot U}{R_t} \quad (A3)$$

$$\omega_r = \omega_t \cdot K_g. \quad (A4)$$

Real and reactive power supplies from the grid side converter to the PCC are given as

$$[P]_{gabc} = \text{real} \left\{ [V\angle\delta]_{abc} \cdot \left(\frac{[V\angle\delta]_{abc} - [V\angle\delta]_{gabc}}{[Z]_{gabc}} \right)^* \right\} \quad (A5)$$

$$[Q]_{gabc} = \text{image} \left\{ [V\angle\delta]_{abc} \cdot \left(\frac{[V\angle\delta]_{abc} - [V\angle\delta]_{gabc}}{[Z]_{gabc}} \right)^* \right\}. \quad (A6)$$

The induction machine's slip is converted to different symmetrical component networks as follows:

$$[s]_{012} = \begin{bmatrix} 0 \\ s \\ 2-s \end{bmatrix}. \quad (A7)$$

Converted sequence network impedances are

$$Z_{s\varepsilon} = Z_s \quad (A8)$$

$$Z_{r0} = \text{infinite} \quad (A9)$$

$$Z_{r1} = \frac{\text{real}(Z_r)}{s_1} + \text{imag}(Z_r) \quad (A10)$$

$$Z_{r2} = \frac{\text{real}(Z_r)}{s_2} + \text{imag}(Z_r) \quad (A11)$$

$$Z_{m\varepsilon} = Z_m. \quad (A12)$$

Induced emf at the stator is written as follows:

$$\bar{E}_\varepsilon = \frac{(\bar{V}_{s\varepsilon}/Z_{s\varepsilon}) + ((\bar{V}_r/s_\varepsilon)/Z_{r\varepsilon})}{1/Z_{s\varepsilon} + 1/Z_{r\varepsilon} + 1/Z_{m\varepsilon}} \quad \varepsilon \neq 0. \quad (A13)$$

The currents on sequence networks are described from

$$\bar{I}_{s\varepsilon} = (\bar{V}_{s\varepsilon} - \bar{E}_\varepsilon)/Z_{s\varepsilon} \quad (A14)$$

$$\bar{I}_{r\varepsilon} = (\bar{V}_{r\varepsilon}/s_\varepsilon - \bar{E}_\varepsilon)/Z_{r\varepsilon} \quad \varepsilon \neq 0 \quad (A15)$$

$$\bar{I}_{r0} = 0. \quad (A16)$$

The relationship of real power balance is described as

$$PL_\varepsilon = |\bar{I}_{s\varepsilon}|^2 \cdot \text{real}(Z_{s\varepsilon}) + |\bar{I}_{r\varepsilon}|^2 \cdot \text{real}(Z_{r\varepsilon}) \quad (A17)$$

$$P_{s\varepsilon} = \text{real}(\bar{V}_{s\varepsilon} \cdot \bar{I}_{s\varepsilon}^*) \quad (A18)$$

$$P_{r\varepsilon} = \text{real}(\bar{V}_{r\varepsilon} \cdot \bar{I}_{r\varepsilon}^*) \quad (A19)$$

and real power balance at any phase

$$\sum_\varepsilon (P_{s\varepsilon} + P_{r\varepsilon}) = P_m/3 + \sum_\varepsilon PL_\varepsilon. \quad (A20)$$

The real and the reactive power output of the WG are

$$[P]_{abc} = [P]_{sabc} + [P]_{gabc} \quad (A21)$$

$$[Q]_{abc} = [Q]_{sabc} + [Q]_{gabc} = 0. \quad (A22)$$

Combining (A1)–(A22), it is possible to form a matrix set of equations as follows:

$$0 = F[U, [V]_{abc}, [\delta]_{abc}, [P]_{abc}, [Q]_{abc}]. \quad (A23)$$

Equation (A23) may be solved with the knowledge of P_m and $[V \angle \delta]_{abc}$ to determine $[P]_{abc}$ and $[Q]_{abc}$ using Newton-Raphson technique.

B. Artificial Neural Network Training Algorithm [19]

When the normalized inputs are fed to the input layer, the error ($E_{rT,j}$) of the j th neuron in output layer (T) compared with the normalized target output (y_j) is estimated as

$$E_{rT,j} = \left. \frac{\partial f_{T,j}(x)}{\partial x} \right|_{n_{sT,j}} (x_{T,j} - y_j). \quad (B1)$$

The propagated errors of the hidden layers are estimated as

$$E_{r_{k-1,i}} = \left. \frac{\partial f_{k-1,i}(x)}{\partial x} \right|_{n_{sk-1,i}} \sum_j w_{k-1,k,i,j} \cdot E_{r_{k,j}}. \quad (B2)$$

The weights are updated in order to minimize the error at the output layer. The updating formula is given in (B3):

$$w_{k-1,k,i,j}^{n+1} = w_{k-1,k,i,j}^n + \eta E_{r_{k,j}}^{n+1} x_{k-1,i}^{n+1} \quad (B3)$$

where n is the iteration count. The MAE, the AAE, the ARMSE are estimated by (B4), (B5), and (B6), respectively:

$$\text{MAE} = \max |x_{T,j} - y_j| \quad \forall e, j \quad (B4)$$

$$\text{AAE} = \frac{\sum_{j=1}^{N_{out}} \left(\sum_{e=1}^{N_e} \frac{|x_{T,j} - y_j|}{N_e} \right)}{N_{out}} \quad (B5)$$

$$\text{ARMSE} = \frac{\sum_{j=1}^{N_{out}} \left(\sum_{e=1}^{N_e} \frac{(x_{T,j} - y_j)^2}{N_e} \right)}{N_{out}} \quad (B6)$$

REFERENCES

- [1] E. R. Ramos, A. G. Expósito, and G. Á. Cordero, "Quasi-coupled three-phase radial load flow," *IEEE Trans. Power Syst.*, vol. 19, no. 2, pp. 776–781, May 2004.
- [2] C. Opathella, B. Venkatesh, and A. Dukpa, "Probabilistic voltage solution method for distribution systems with wind electric generators," in *Proc. 2010 IPEC Conf.*, pp. 220–223.
- [3] J. M. Morales, A. J. Conejo, and J. Perez-Ruiz, "Simulating the impact of wind production on locational marginal prices," *IEEE Trans. Power Syst.*, vol. 26, no. 2, pp. 820–828, May 2011.
- [4] S. Khushalani, J. M. Solanki, and N. N. Schulz, "Development of three-phase unbalanced power flow using PV and PQ models for distributed generation and study of the impact of DG models," *IEEE Trans. Power Syst.*, vol. 22, no. 3, pp. 1019–1025, Aug. 2007.
- [5] J.-H. Teng, "Modeling distributed generations in three-phase distribution load flow," *IET Gen., Transm., Distrib.*, vol. 2, no. 2, pp. 330–340, Jul. 2008.
- [6] A. E. Feijoo and J. Cidras, "Modeling of wind farms in the load flow analysis," *IEEE Trans. Power Syst.*, vol. 15, no. 1, pp. 110–115, Feb. 2000.
- [7] A. Feijoo, "On PQ models for asynchronous wind turbines," *IEEE Trans. Power Syst.*, vol. 24, no. 4, pp. 1890–1891, Nov. 2009.
- [8] U. Eminoglu, "Modeling and application of wind turbine generating system (WGS) to distribution systems," *Renew. Energy*, vol. 34, no. 11, pp. 2474–2483, Mar. 2009.
- [9] K. C. Divya and P. S. N. Rao, "Models for wind turbine generating systems and their application in load flow studies," *Elect. Power Syst. Res.*, vol. 76, no. 9–10, pp. 844–856, Jun. 2006.
- [10] J. F. M. Padron and A. E. F. Lorenzo, "Calculating steady-state operating conditions for doubly-fed induction generator wind turbines," *IEEE Trans. Power Syst.*, vol. 25, no. 2, pp. 922–928, May 2010.
- [11] R. Jayashri and R. P. K. Devi, "Steady state analysis of wind turbine generators interconnected to the grid," in *Proc. 2006 IEEE Power Engineering Society Power Systems Conf. Expo.*, pp. 1273–1279.
- [12] G. Ofner, O. Koenig, G. Dannerer, and R. Seebacher, "Steady state modeling of doubly fed induction generators for mega watt class wind turbines," in *Proc. 2010 XIX Int. Electrical Machines Conf.*, pp. 1–6.

- [13] J. G. Slootweg, H. Polinder, and W. L. Kling, "Representing wind turbine electrical generating systems in fundamental frequency simulations," *IEEE Trans. Energy Convers.*, vol. 18, no. 4, pp. 516–524, Dec. 2003.
- [14] B. Babypriya and R. Anita, "Modeling, simulation and analysis of doubly fed induction generator for wind turbines," *J. Elect. Eng.*, vol. 60, no. 2, pp. 79–85, 2009.
- [15] Z. Chen and E. Spooner, "Grid interface options for variable-speed permanent magnet generators," in *Proc. 1998 IEE Electric Power Applications Conf.*, pp. 273–283.
- [16] A. Dadhania, "Modeling of doubly fed induction generators for distribution system load flow analysis," M.A.S. thesis, Dept. Elect. Comput. Eng., Univ. Ryerson, Toronto, ON, Canada, 2010.
- [17] I. S. Wander, "Modeling of synchronous generator and full-scale converter for distribution system load flow analysis," M.A.S. thesis, Dept. Elect. Comput. Eng., Univ. Ryerson, Toronto, ON, Canada, 2011.
- [18] S. Li, D. C. Wunsch, E. A. O'Hair, and M. G. Giesselmann, "Using neural networks to estimate wind turbine power generation," *IEEE Trans. Power Syst.*, vol. 16, no. 2, pp. 276–282, May 2001.
- [19] K. L. Priddy and P. E. Keller, *Artificial Neural Networks an Introduction*. Bellingham, WA: SPIE—Int. Soc. Opt. Eng., 2005, pp. 110–116.
- [20] IEEE Power Engineering Society, "Distribution Test Feeders," –37 bus feeder. [Online]. Available: <http://ewh.ieee.org/soc/pes/dsacom/testfeeders/index.html>.
- [21] W. H. Kersting, *Distribution System Modeling and Analysis*. Boca Raton, FL: CRC, 2002.

C. Opathella (S'10) received the B.Sc. degree in electrical engineering from University of Moratuwa, Sri Lanka, in 2003 and the M.Eng. degree in energy economics and planning from the Asian Institute of Technology, Thailand. He is currently pursuing the Ph.D. degree in Ryerson University, Toronto, ON, Canada.

His research interests are power system planning, optimization, and renewable energy integration into the power system.

B. N. Singh received the B.Eng. degree in 1979 and the M.Eng. degree in 1984 from Memorial University of Newfoundland, Canada.

His three decades of work experience covers system planning (T&D), protection and control design, and engineering standards. He is currently Manager, Asset Management and works in the areas of long-term grid planning, smart grid implementation, and R&D.

D. Cheng (M'77) received the Ph.D. degree from the University of Manchester, Manchester, U.K.

He held various senior engineering positions in the U.K. and Singapore Electric Grid businesses for more than 20 years. He is currently a Post Doctoral Fellow of the Centre of Urban Energy at Ryerson University, Toronto, ON, Canada. His research interests are in power system planning, analysis, and optimization.

B. Venkatesh (M'95–SM'08) received the Ph.D. degree from Anna University, Chennai, India, in 2000.

He is an Associate Professor and Academic Director of the Centre of Urban Energy at Ryerson University, Toronto, ON, Canada. His research interests are power system analysis and optimization.